Journal of Pharmacological and Toxicological Methods xxx (2016) xxx–xxx

Contents lists available at ScienceDirect

Journal of Pharmacological and Toxicological Methods

journal homepage: www.elsevier.com/locate/jpharmtox

Research article

Cardiotoxicity screening with simultaneous optogenetic pacing, voltage imaging and calcium imaging

Graham T. Dempsey [a], Khuram W. Chaudhary [b,*], Nicholas Atwater [a], Cuong Nguyen [a], Barry S. Brown [b], John D. McNeish [c], Adam E. Cohen [d,e,f], Joel M. Kralj [a]

[a] Q-State Biosciences, Cambridge, MA, USA
[b] GlaxoSmithKline-Safety Assessment, King of Prussia, PA, USA
[c] GlaxoSmithKline-Alternative Discovery and Development, Cambridge, MA, USA
[d] Department of Physics, Harvard University, Cambridge, MA, USA
[e] Department of Chemistry and Chemical Biology, Harvard University, Cambridge, MA, USA
[f] Howard Hughes Medical Institute, Chevy Chase, MD, USA

ARTICLE INFO

Article history:
Received 2 February 2016
Received in revised form 2 May 2016
Accepted 9 May 2016
Available online xxxx

Keywords:
Cardiomyocytes
Cardiotoxicity
Channelrhodopsin
Comprehensive *in vitro* Proarrhythmia Assay
Human induced pluripotent stem cells
Methods
Optogenetics
Pacing
Torsades de Pointes
Voltage indicator

ABSTRACT

Introduction: The Comprehensive *in vitro* Proarrhythmia Assay (CiPA) initiative seeks an *in vitro* test to accurately predict clinical Torsades de Pointes (TdP). We developed a cardiotoxicity assay incorporating simultaneous measurement of the action potential (AP) waveform and Ca^{2+} transient (CT) in human iPSC-derived cardiomyocytes (CMs). Concurrent optogenetic pacing provided a well-controlled electrophysiological background.
Methods: We used the Optopatch platform for all-optical electrophysiology (Hochbaum et al., 2014). In a monolayer culture, a subset of cells expressed a genetically encoded, calcium and voltage reporter, CaViar (Hou, Kralj, Douglass, Engert, & Cohen, 2014), while others expressed a channelrhodopsin variant, CheRiff. Optical pacing of CheRiff-expressing cells synchronized the syncytium. We screened 12 compounds (11 acute, 1 chronic) to identify electrophysiological (AP rise time, AP50, AP90, beat rate) and CT effects in spontaneously beating and paced cultures (1 Hz, 2 Hz).
Results: CaViar reported spontaneous and paced APs and CTs with high signal-to-noise ratio and low phototoxicity. Quinidine, flecainide, E-4031, digoxin and cisapride prolonged APs, while verapamil and nifedipine shortened APs. Early after depolarizations (EADs) were elicited by quinidine, flecainide and cisapride. All but four compounds (amiodarone, chromanol, nifedipine, verapamil) prolonged AP rise time. Nifedipine and verapamil decreased CT amplitude, while digoxin increased CT amplitude. Pentamidine prolonged APs after chronic exposure.
Discussion: The Optopatch platform provides a robust assay to measure APs and CTs in hiPSC-CMs. This addresses the CiPA mandate and will facilitate comparisons of cell-based assays to human clinical data.

1. Introduction

Toxicity accounts for 20% of all drug attrition, of which, approximately one third is cardiovascular (Guengerich, 2011). Drug induced abnormalities in the electrocardiogram (ECG), which can lead to sudden death, account for nearly half of these failures (Stevens & Baker, 2009). Because the cost of bringing a novel chemical entity to market can exceed $1.2 billion, along with >10 years of research and development, it is critical to address and eliminate cardiovascular toxicity early in development (Adams & Brantner, 2010; Stevens & Baker, 2009).

A major focus in reducing cardiotoxicity has been to identify compounds that cause acquired long QT syndrome. A causal link exists between QT prolongation and increased incidence of the potentially lethal arrhythmia, TdP (Coumel, Leclercq, & Lucet, 1985; Keating, 1995; Roden et al., 1996). As our understanding of electrophysiological mechanisms for QT prolongation has increased, especially the propensity of hERG potassium channel blockade to cause long QT and TdP, regulators have created guidance documents (ICHS7A/B) to characterize the *in vitro* and *in vivo* consequences of this property (Haverkamp et al., 2000; ICHS7B, 2005; Sanguinetti, Jiang, Curran, & Keating, 1995; Zhou et al., 1998).

Studies on clinically relevant compounds have shown that hERG inhibition is not always predictive of QT prolongation and torsadogenic potential (Lu et al., 2008; Redfern et al., 2003). While selective hERG

Abbreviations: CiPA, Comprehensive *in vitro* Proarrhythmia Assay; TdP, Torsades de Pointes; AP, action potential; CT, Ca^{2+} transient; hiPSC, human induced pluripotent stem cell; CM, cardiomyocyte; CaViar, Ca^{2+} and voltage indicator; CheRiff, channelrhodopsin variant; EAD, early after depolarization; ECG, electrocardiogram; hERG, human Ether-à-go-go-Related Gene; MEA, multi-electrode array; Arch, Archaerhodopsin; VSD, voltage sensitive dye.

* Corresponding author.
E-mail address: khuram.w.chaudhary@gsk.com (K.W. Chaudhary).

http://dx.doi.org/10.1016/j.vascn.2016.05.003
1056-8719/

blockers tend to prolong the QT/QTc interval when unbound plasma concentrations fall within 30–100 fold of their hERG IC_{50}, several compounds exist in this concentration range yet elicit little to no change in QTc (Gintant, 2011; Redfern et al., 2003). Compounds such as ranolazine and verapamil are often cited to refute the sole use of hERG potency in making predictions of QT, because they block depolarizing currents in a manner that compensates for hERG block, rendering these compounds clinically safe (Chouabe, Drici, Romey, Barhanin, & Lazdunski, 1998; De Ponti, Poluzzi, Cavalli, Recanatini, & Montanaro, 2002; Schram et al., 2004; Song, Shryock, Wu, & Belardinelli, 2004). These examples clearly illustrate the shortcomings of simplifying AP prolongation to the liability against a single ion channel and highlight the need for more physiologically relevant *in vitro* platforms.

Pre-clinical *in vivo* models can provide relatively strong concordance with human QT interval, as is the case for QTc comparisons between canines and humans; whereas other *in vitro* models lack the sensitivity or are prone to technical artifacts (Hanson et al., 2006; Holzgrefe et al., 2014). In a retrospective analysis, approximately 80% of cardiotoxicities were identified by animal studies (including ECG abnormalities), whereas assays such as the dog Purkinje fiber have shown correlations as low as 33% (Hanson et al., 2006; Olson et al., 2000). Each of these *in vitro* preparations provides insight into the mechanism of toxicity, yet falls short of recapitulating the human condition. Regulatory guidelines acknowledge the investigative nature of the surrogate *in vitro* assays and accommodate incorporation of new assays.

The advent of stem cell-derived CMs has revolutionized our ability to study human cardiac physiology *in vitro*. CMs derived from human embryonic and inducible pluripotent stem cells express myofilament proteins and have electrophysiological properties similar to primary myocytes (Doevendans et al., 2000; Ribeiro et al., 2015). These cells express cardiac ion channels, produce APs resembling the atrial, nodal and ventricular myocytes, and create spontaneously beating tissues (He, Ma, Lee, Thomson, & Kamp, 2003; Ma et al., 2011; Mummery et al., 2003; Vanderlaan, Oudit, & Backx, 2003; Wang et al., 2014). HiPSCs can now be differentiated into cultures that are predominantly (95%) cardiomyocytes. Early measurements based on small numbers of cells reported mixed populations with action potential waveforms indicative of ventricular, atrial and nodal cells (Burridge et al., 2014; Lan et al., 2013; Puppala et al., 2013). More recent measurements with voltage-sensitive dyes suggested a continuous distribution of AP morphologies, with a dependence on cell density (Du, Hellen, Kane, & Terracciano, 2015).

Studies have shown that hiPSC-derived CMs exhibit sensitivity to ion channel inhibitors by replicating characteristic changes in AP duration (Honda, Kiyokawa, Tabo, & Inoue, 2011; Ma et al., 2011). These innovations have changed the landscape of pre-clinical cardiotoxicity screening such that regulatory agencies are considering the use of hiPSC-derived CMs as an early screen for proarrhythmic risk (Cavero & Holzgrefe, 2014; Himmel, 2013; Sager, Gintant, Turner, Pettit, & Stockbridge, 2014). As stem cell technologies evolve, it is important to recognize their utility and limitations, especially as they relate to clinical translation.

ECG arrhythmias are by definition electrical, so assays must measure electrical activity of CMs when screening for proarrhythmic risk. While current-clamp electrophysiology provides the gold standard of AP measurement, it requires specialized skill, is labor intensive and low-throughput. Thus, researchers have studied the use of multi-electrode arrays (MEA) to recreate a pseudo-ECG from a monolayer of hiPSC-derived CMs to measure field potential duration and electrical conduction (Caspi et al., 2009; Guo et al., 2011). The monolayer of cells behaves as a syncytium much like cardiac tissue; however, the cells are unpaced. Beat rate is a critical determinant of AP duration and rate-associated changes in AP waveform can mask more subtle drug effects. Further, it is difficult to qualify the nature of proarrhythmic events, such as early *versus* delayed after depolarizations. MEA provides neither single-cell resolution nor calcium data.

Here, we describe a novel optogenetic technique for simultaneous optical pacing, voltage imaging and calcium imaging in a syncytial culture of hiPSC-derived CMs. Pacing is achieved through optogenetic stimulation of a subset of the cells. These cells synchronize the syncytium through gap junction-mediated conduction. Readout is achieved through expression of reporter proteins in a disjoint subset of the cells. By segregating the paced cells from the readout cells, we ensure that the recordings are free of stimulus artifacts.

Pacing of CMs is achieved through the use of a channelrhodopsin variant called CheRiff (Hochbaum et al., 2014). CheRiff, derived from a freshwater alga, has been shown to trigger APs in neurons with approximately 9-fold lower blue light intensity than is required for the widely used Channelrhodopsin 2 H134R actuator (Hochbaum et al., 2014). We show that optical stimulation of CheRiff expressed in a subset of CMs can pace the entire syncytium through gap junction-mediated electrical conduction.

Detection of AP and CT waveforms was accomplished through the use of a fusion protein called CaViar (for 'Ca^{2+} and voltage indicator' (Hou, Kralj, Douglass, Engert, & Cohen, 2014)) consisting of a red-light-excited voltage indicating fluorescent protein, QuasAr2 (Hochbaum et al., 2014) with a blue-light-excited Ca^{2+} indicating protein, GCaMP6f (Chen et al., 2013). The QuasAr2 and GCaMP6f constructs have each been thoroughly characterized individually as well as in combination in the CaViar construct (Hou et al., 2014). QuasAr2 has a rapid response time (0.3 ms at 34 °C), high intrinsic sensitivity to voltage changes (90% ΔF/F per 100 mV), although imperfect trafficking in some cells reduces the effective sensitivity to 10–30% per 100 mV, no photocurrent (Hochbaum et al., 2014) and negligible capacitive load (Maclaurin, Venkatachalam, Lee, & Cohen, 2013). In neurons, expression of QuasAr2 did not perturb resting voltage, membrane resistance, membrane capacitance, AP initiation voltage or AP waveform (Hochbaum et al., 2014).

The GCaMP6f indicator responds to Ca^{2+} with a fluorescence dynamic range of 52:1, a K_d of 375 nM, a Hill coefficient of 2.3 and an Ca^{2+} off-rate of 3.9 s^{-1} (Chen et al., 2013). This sensor has been used for high-resolution mapping of Ca^{2+} dynamics in hiPSC-derived CMs (Huebsch et al., 2014). In primary CM, a membrane-targeted version of the sensor showed 4-fold faster kinetics than the cytoplasmic variant, and was shown not to disrupt endogenous Ca^{2+} handling (Kaestner et al., 2014; Shang et al., 2014). The linker in the CaViar construct has been optimized to eliminate steric interactions or energy transfer between the GCaMP6f and the QuasAr2. CaViar has been used to map simultaneous propagation of APs and CTs in embryonic zebrafish hearts *in vivo* (Hou et al., 2014).

The combination of the CheRiff actuator and CaViar reporter form the basis of the platform we call Cardiac Optopatch. To test Cardiac Optopatch as a platform for cardiotoxicity screening, the effects of eleven compounds were measured at the endogenous beat rate and at two optically stimulated rates. Pentamidine was tested under chronic conditions, demonstrating the ability of long-term measurements. This study provides a benchmark for rapidly evaluating cardiotoxic effects, including AP morphology, kinetics and CTs, of clinically relevant compounds in an optically paced cardiomyocyte preparation using fluorescent proteins.

2. Methods

2.1. Cell culture and transduction with Cardiac Optopatch vectors

iCell® Cardiomyocytes, Cellular Dynamics Inc. (CDI) were cultured in six-well plates following manufacturer instructions. Five days after plating, hiPSC-derived CMs were transduced overnight with custom made lentiviral vectors for either CaViar and/or CheRiff. Virus was removed from the cells and 1.5 mL of maintenance medium added to each well. The efficiency of viral delivery was ~90%.

Please cite this article as: Dempsey, G.T., et al., Cardiotoxicity screening with simultaneous optogenetic pacing, voltage imaging and calcium imaging, *Journal of Pharmacological and Toxicological Methods* (2016), http://dx.doi.org/10.1016/j.vascn.2016.05.003

For voltage imaging, CaViar and CheRiff-expressing cells were resuspended, mixed and replated onto glass-bottom imaging wells. Dishes (MatTek; 10 mm glass diameter, #1.5) were coated with 10 μg/mL fibronectin (Sigma-Aldrich) in 0.1% gelatin overnight at 4 °C. Cells expressing CaViar and CheRiff were trypsinized according to the manufacturer's protocol, mixed at a ratio of 5:1 CaViar:CheRiff, and then pelleted. The combined cells were then re-suspended in 2.1 mL of maintenance medium and plated overnight at a density of 8.5×10^4 cells/cm^2 in 100 μL of plating medium. Maintenance medium (1.0 mL) was added to each dish and the cells were fed every 48 h.

For simultaneous voltage and Ca^{2+} imaging, CheRiff-expressing cells were replated in the periphery of each imaging chamber, with CaViar cells replated in the center. MatTek dishes were prepared to segregate CheRiff-expressing cells from CaViar-expressing cells. 8 mm-diameter poly-dimethylsiloxane (PDMS) discs were treated with 10 μg/mL fibronectin in 0.1% gelatin on one side for 10 min at room temperature. The discs were dried and pressed onto the MatTek dish glass surface, slightly offset. The remaining area of the glass was coated with 10 μg/mL fibronectin in 0.1% gelatin and left overnight. Cells expressing the CheRiff were trypsinized according to the manufacturer's protocol and re-suspended in 50 μL of maintenance medium per dish. For plating, 50 μL of the CheRiff cells were added to the exposed glass surface and allowed to sit for 40 min at 37 °C in 5% CO_2. The PDMS discs were removed, the glass surface washed with 150 μL of maintenance medium and the remaining volume aspirated. Trypsinized CaViar cells were then re-suspended in 100 μL of maintenance medium per dish and plated overnight at a density of 7.0×10^4 cells/cm^2. 1.0 mL of maintenance medium was added to each dish and the cells were fed every 48 h.

2.2. Sample treatment prior to imaging

Cells were imaged 5–7 days post-replating (12–14 days post-thaw). Prior to imaging, cells were incubated with 5 μM retinal in maintenance medium for >30 min at 37 °C in 5% CO_2. Exogenous retinal is added to the dishes to ensure that all QuasAr2 proteins contain the chromophore in the event that inadequate retinal is supplied in the cellular media. Retinal-containing medium was removed from the dish and 1.5 mL of warmed maintenance medium without phenol red, vitamins and amino acids (referred to as cardiac imaging buffer) was added. Cells were kept at 37 °C in 5% CO_2 for 30 min prior to imaging.

2.3. Preparation and storage of drug stocks and dilutions

Drugs were purchased as dried powders (Sigma-Aldrich). Compounds were dissolved in DMSO, with the exception of E-4031 which was dissolved in H_2O, at a stock concentration of 10 mM. Compounds were solubilized by vortexing the solution at room temperature until dissolved. Stock solutions were stored at −20 °C until use. Immediately prior to use, drugs were diluted in cardiac imaging buffer. Addition of 100 μL of diluted stock to the dish achieved the final drug concentration. A blank containing cardiac imaging buffer alone was prepared for each drug. Drugs were kept at 37 °C in 5% CO_2 prior to use.

2.4. Spontaneous beating and paced action potentials

CMs expressing CaViar were exposed to whole-field illumination with red laser light ($\lambda = 640$ nm, 50 W/cm^2) to excite fluorescence of QuasAr2. Fluorescence was collected *via* a 20× water immersion objective with a numerical aperture (NA) of 1.0 through a Cy5 emission filter (Chroma). Signals were recorded on a sCMOS camera (Hamamatsu) at frame rates of 100 Hz or 500 Hz. Pulses of blue LED illumination (6 ms, 0.5 W/cm^2, $\lambda = 488$ nm) stimulated CheRiff, which paced the entire syncytium through gap junction-mediated conduction.

2.5. Simultaneous imaging of voltage and Ca^{2+}

Pulses of blue LED illumination (6 ms, 0.5 W/cm^2, $\lambda = 488$ nm) stimulated CheRiff in the peripheral cells to pace the syncytium. Blue laser light ($\lambda = 488$ nm, 0.15 W/cm^2) excited fluorescence of GCaMP6f in the central cells. Red laser light ($\lambda = 640$ nm, 50 W/cm^2) excited fluorescence of QuasAr2 in the central cells. A dual-view imaging system projected emission from GCaMP6f (525–575 nm) and from QuasAr2 (660–760 nm) onto adjacent halves of a sCMOS camera, operating at a frame rates of 100 Hz or 500 Hz.

2.6. Drug measurements

Imaging was performed on a custom-built epi-fluorescence microscope. Cells were maintained at a temperature of 35–37 °C using a heated stage (Warner Instruments) and objective collar (Bioptechs). A home-built environmental chamber maintained 100% humidity and 5% CO_2.

The imaging protocol comprised measurement of spontaneous activity (30 s), immediately followed by activity under 1 Hz and 2 Hz pacing (15 s each), repeated in three fields of view (FOV). Drug addition started with a blank, followed by within-dish dose-escalation. A vehicle control was performed for DMSO at concentrations of 0.003%, 0.01%, 0.03%, 0.1% and 0.3%.

2.7. Analysis

Voltage traces were first corrected for photobleaching using a sliding linear interpolation with a 2 s window. Each trace was scaled to report fractional changes in fluorescence relative to baseline (ΔF/F). The first derivative of each trace was used to locate the spike upstroke (maximal dF/dt). In paced recordings, blue light stimulus artifacts were removed by linear interpolation between the frames immediately before and after the stimulus pulse. There was typically a 10 ms delay between the onset of the blue pulse and the upstroke of the AP. Ca^{2+} traces were not corrected for photobleaching. The spike timing was extracted using the information from the voltage traces. Each Ca^{2+} trace was scaled to fractional fluorescence units, ΔF/F.

The inter-beat interval was calculated by recording the average time, in seconds, between AP upstrokes, whose timing was determined as described above. AP50 and AP90 were calculated from the average beat from each 100 Hz frame-rate movie. The AP width was the time between crossing 50% (or 10%) of the maximum fluorescence deviation on the upstroke and the downstroke. Linear interpolation was used to achieve sub-frame precision. The rise time was determined from 500 Hz movies. The upstroke was defined as the time for the fluorescence to travel between 30 and 70% of the full swing. Timing was calculated with sub-frame precision using linear interpolation. The reported value was the mean rise time over all beats in a given trace. The Ca^{2+} transient was characterized by the amplitude of ΔF/F in the CT, averaged over all beats in a given trace.

All error bars reported represent the standard error of the mean across three FOV acquired in each of two dishes unless indicated otherwise. All statistical comparisons were performed using a one-way ANOVA with Dunnett's test for statistical significance. All *P* values are considered significant if <0.05.

3. Results

3.1. QuasAr2 accurately and non-perturbatively reports AP waveforms

We first tested the capability of QuasAr2 to report AP waveforms by comparing with a highly sensitive VSD, FluoVolt (Miller et al., 2012). QuasAr2 was expressed under control of the CMV promoter in a subset of hiPSC-derived CMs and all cells were labeled with FluoVolt. The two

Please cite this article as: Dempsey, G.T., et al., Cardiotoxicity screening with simultaneous optogenetic pacing, voltage imaging and calcium imaging, *Journal of Pharmacological and Toxicological Methods* (2016), http://dx.doi.org/10.1016/j.vascn.2016.05.003

reporters absorb and emit at different wavelengths, so their signals were readily separated and recorded simultaneously (Fig. 1).

Spontaneously beating cells expressing QuasAr2 and labeled with FluoVolt showed bursts of fluorescence from each reporter, synchronous with the beating. To test whether QuasAr2 accurately reported the underlying AP waveform, we compared the FluoVolt and QuasAr2 signals recorded from the same cell. The two waveforms showed good correspondence (<2% difference in AP50; Fig. 1A). To test whether expression of QuasAr2 affected the AP waveform, we compared FluoVolt signals in neighboring cells ± QuasAr2 expression. The FluoVolt waveform showed no detectable difference between cells ± QuasAr2 (Fig. 1A).

Because QuasAr reporters require high illumination intensity, we tested for photobleaching or phototoxicity arising from imaging of QuasAr2 in CMs. Fig. 1B shows the QuasAr2 fluorescence during 500 s of continuous red laser illumination (50 W/cm^2), with baseline drift removed. The signal amplitude decreased by 12% during the acquisition and showed a modest shortening of the AP50 (199 ms to 192 ms) and AP90 (318 ms to 307 ms). This level of variability in AP width is within the natural variation in spontaneously beating hiPSC-derived CMs.

3.2. CheRiff and CaViar form the Optopatch system to optically stimulate and record voltage and Ca^{2+} in hiPSC-derived CMs

To avoid artifacts from non-specific channelrhodopsin conductance, cell expressing CheRiff alone were used to pace the syncytium. For detection of AP waveform alone, cells expressing CheRiff and cells expressing CaViar were intermixed (Fig. 2). For detection of APs and CTs, CheRiff-expressing cells were plated to the side of the syncytium, to avoid spurious CheRiff activation by the blue light used to excite GCaMP6f (Fig. 2B). Fig. 2C shows simultaneously recorded single-trial fluorescence time traces for QuasAr2 and GCaMP6f, without filtering or other post-processing. AP and CT waveforms could be detected for spontaneous or paced beating at 1 Hz and 2 Hz.

3.3. Cardiac Optopatch as a platform for cardiotoxicity testing

We next tested the effects of drugs on cardiac AP dynamics at 37 °C. We measured voltage transients in 8–10 cells per FOV, at three pacing rates, three FOVs per dish, six drug concentrations (1 'blank' with no drug and 5 drug concentrations) and two dishes. The duplication over dishes was to control for dish-to-dish variation.

Dish-to-dish variability across all of the studies was quantified using 'blank' measurements made immediately prior to compound addition. Fig. 3 shows average AP and CT waveforms as well as dot density plots comparing AP50, AP90, beat rate and rise time for spontaneously beating cultures and cultures paced at 1 Hz and 2 Hz. The pacing shortened the AP in a rate-dependent manner and decreased dish-to-dish variability in AP parameters (Fig. 3C). The AP50 was 391 ± 61 ms (mean ± s.d.) in spontaneously beating cultures, 293 ± 24 ms at 1 Hz pacing and 191 ± 17 ms at 2 Hz pacing. AP90 showed a similar trend (528 ± 79 ms for spontaneous beating, 422 ± 40 ms for 1 Hz pacing, 293 ± 23 ms for 2 Hz pacing), as did the rise time, but only at 2 Hz pacing (3.9 ± 1.0 ms for spontaneous beating, 3.3 ± 1.1 ms for 1 Hz pacing, 2.8 ± 0.4 ms for 2 Hz pacing). The dot density plot is also shown for the spontaneous beat rate of the cultures (32.1 ± 7.6 beats/min).

Cells followed the specified pacing regime, and voltage changes were detected with fractional fluorescence changes of ΔF/F = 30% and high signal-to-noise ratio (500:1 at 100 Hz frame rate; 200:1 at 500 Hz frame rate). In the un-paced culture, the AP width showed an apparent decrease with increasing DMSO concentration: from 0% to 0.3% DMSO, AP50 decreased from 464 ± 11 ms to 394 ± 8 ms and AP90 decreased from 600 ± 23 ms to 512 ± 15 ms (not shown). However, these results are explained by the increase in the spontaneous beat rate from 25.8 ± 0.9 to 28.8 ± 2.4 beats/min over the course of 75 min measurement. Under optical pacing conditions, the fractional changes in AP parameters were approximately three-fold smaller: at 1 Hz from 0% to 0.3% DMSO, AP50 decreased from 315 ± 8 ms to 292 ± 10 ms and AP90 decreased from 439 ± 20 ms to 408 ± 19 ms.

3.4. Acute drug effects on AP waveform as measured by Cardiac Optopatch

To characterize pharmacological effects on APs, we tested compounds with known mechanisms, including several hERG K^+ and Na^+ channel blockers, as well as some with multiple targets. A summary of the effects of compound addition on voltage dynamics is shown in Table 1, as determined using Optopatch.

Cisapride is a gastroprokinetic removed from the market due to cardiac side effects arising from hERG block (Hennessy, Leonard, Newcomb, Kimmel, & Bilker, 2008). In our Optopatch assay, cisapride

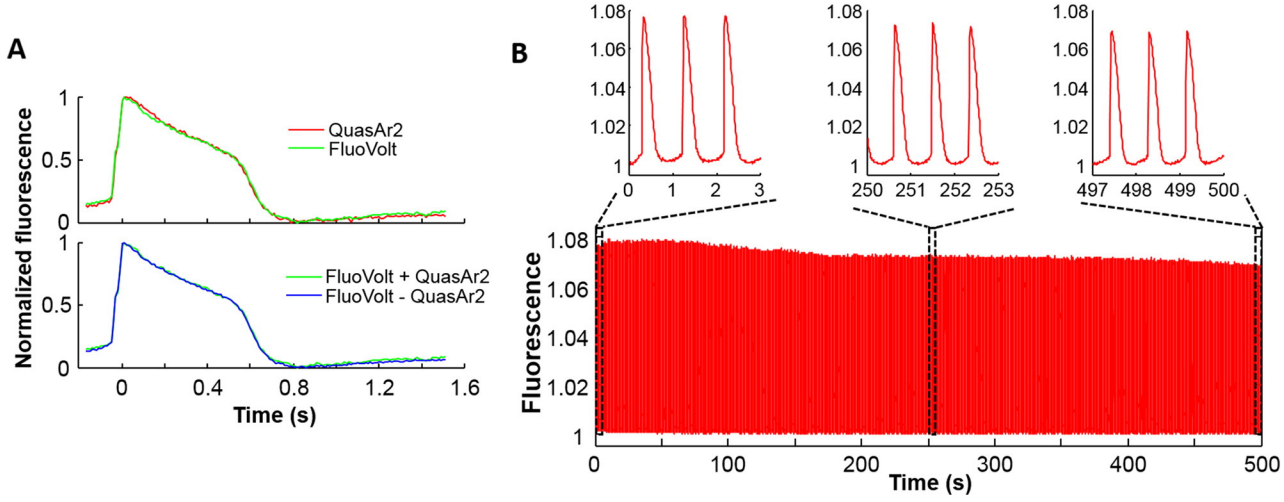

Fig. 1. QuasAr2 reports cardiomyocyte (CM) action potentials (APs). (A) Comparison of the CM AP waveforms, as measured by the genetically encoded voltage indicator QuasAr2 and the voltage-sensitive dye, FluoVolt. Cells were sparsely transfected with the QuasAr2 construct and then treated with FluoVolt dye. QuasAr2 was excited by red laser light with fluorescence detection centered at 720 nm. FluoVolt was excited by 488 nm laser light with fluorescence detection centered at 525 nm. The top panel shows the simultaneously recorded AP waveforms from a cell expressing QuasAr2 (red line) and labeled with FluoVolt (green line). The lower trace compares the FluoVolt AP waveform in the presence (FluoVolt$^+$, QuasAr2$^+$, green) and absence (FluoVolt$^+$, QuasAr2$^-$, cyan) of QuasAr2 expression. (B) Phototoxicity and photobleaching measurement of QuasAr2. Cells were imaged under continuous red laser illumination (~50 W/cm^2) for 500 s. Expanded views of the fluorescence recording are shown in the lower panels. (For interpretation of the references to color in this figure legend, the reader is referred to the web version of this article.)

Please cite this article as: Dempsey, G.T., et al., Cardiotoxicity screening with simultaneous optogenetic pacing, voltage imaging and calcium imaging, *Journal of Pharmacological and Toxicological Methods* (2016), http://dx.doi.org/10.1016/j.vascn.2016.05.003

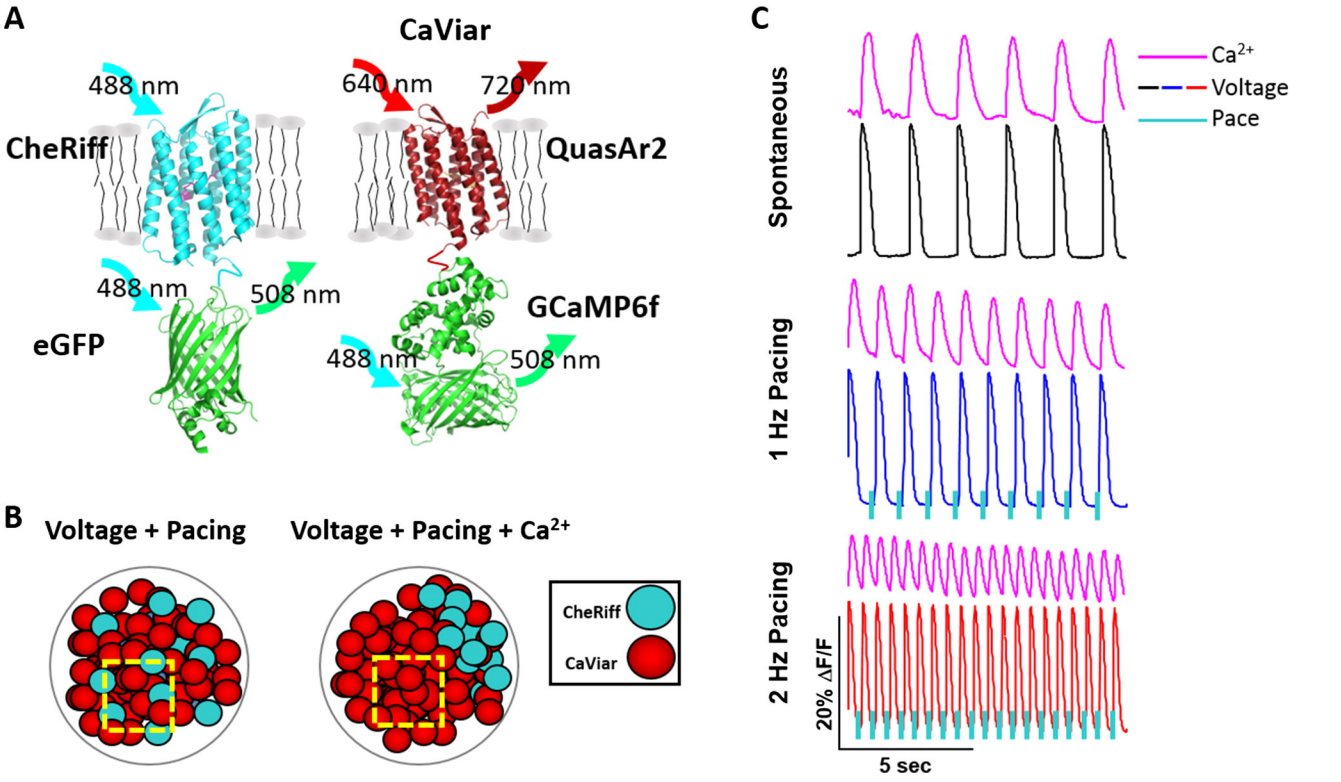

Fig. 2. Optogenetic constructs and plating schemes for simultaneous pacing, voltage and Ca^{2+} measurement. (A) Schematic structures of optogenetic proteins used for pacing and detection of voltage and intracellular Ca^{2+}. The crystal structures of CheRiff and QuasAr2 have not been solved; the diagrams show homologous proteins. Pacing of CMs is achieved through pulsed 488 nm LED illumination of CheRiff. The CheRiff construct is coupled to an eGFP tag for detection of CheRiff expression. A fusion protein called CaViar (Hou et al., 2014), consisting of QuasAr2 (Hochbaum et al., 2014) fused to GCaMP6f (Chen et al., 2013), was used for simultaneous voltage and Ca^{2+} imaging. QuasAr2 was excited *via* red laser light. GCaMP6f was excited *via* blue laser light. Cells were separately transduced with either CheRiff or CaViar vectors. (B) CM plating configurations. For simultaneous optical pacing and voltage imaging, CheRiff cells (solid cyan circles) were co-mingled with CaViar cells (solid red circles). The yellow dotted line indicates a microscope field of view. For simultaneous optical pacing and imaging of both Ca^{2+} and membrane voltage, cells were plated to spatially segregate CheRiff-expressing cells to avoid optical crosstalk. The CheRiff-expressing cells lay outside the imaging region. (C) Voltage traces for spontaneous beating (black), paced beating at 1 Hz (blue) and paced beating at 2 Hz (red). Optical pacing stimuli are shown as cyan dashes. The simultaneous measurement of Ca^{2+} (magenta) is shown at each pacing condition. (For interpretation of the references to color in this figure legend, the reader is referred to the web version of this article.)

had a pronounced effect on the AP waveforms (Fig. 4A, C). Under spontaneous beating, 0.1 μM cisapride increased AP90 (from 536 ± 8 ms to 851 ± 4 ms, Fig. 4C). The spontaneous beat rate remained constant before decreasing sharply at 1 μM. At 1 μM, EADs were observed, along with a dramatic increase in the AP90 to 1200 ± 210 ms (Fig. 4A, C). The effects of additional hERG channel blockers, E-4031 and terfenadine, are summarized in Table 1.

We next tested several Na^+ channel blockers including flecainide (Fig. 4B, D). Flecainide, at 1 Hz pacing, increased the AP90 from 465 ± 7 ms to 616 ± 2 ms at 3 μM (Fig. 4D). The rise time increased from 2.6 ± 0.1 ms to 9.4 ms at 3 μM. At 3 μM, cells showed a cessation of spontaneous beating and at 10 μM stopped beating all together (Fig. 4B). The effects of the Na^+ channel blockers lidocaine and quinidine are summarized in Table 1.

Finally, two drugs showed no effects at any concentrations tested. Amiodarone, which exhibits Class I, II, III and IV properties, showed no significant changes with increasing concentration in either of the measurements. Similarly, chromanol had no effect on the AP waveforms.

3.5. Acute drug effects on AP waveform and CT dynamics as measured by Optopatch

We next tested three compounds using simultaneous measurement of voltage and Ca^{2+}. A summary of the effects of compound addition on voltage and calcium dynamics is shown in Table 1.

As in the voltage-only measurements, DMSO addition showed little effect on the AP waveforms or CTs. The measured amplitude of the calcium transients slightly decreased throughout the experiment due to photobleaching of the GCaMP6f sensor; at 1 Hz pacing the amplitude decreased from ΔF/F = 0.13 ± 0.01 to 0.08 ± 0.01 at 0.3% DMSO. At the spontaneous beat rate, the AP50 decreased from 352 ± 1 ms to 278 ± 7 ms and AP90 decreased from 481 ± 3 ms to 392 ± 4 ms at 0.3% DMSO, respectively. This decrease is consistent with the observed increase in spontaneous beat rate from 34.7 ± 1 bpm to 42.6 ± 1 bpm. This change was smaller in paced cultures. At 1 Hz pacing, the AP50 decreased from 275 ± 2 ms to 252 ± 3 ms at 0.3% DMSO and AP90 decreased from 420 ± 1 ms to 356 ± 2 ms at 0.3% DMSO.

Nifedipine affected voltage and calcium transients in both spontaneously beating and paced cultures (Fig. 5). Most notably, the calcium amplitude showed a decrease from ΔF/F = 0.12 ± 0.02 to 0.08 ± 0.02 under 1 Hz pacing conditions at the lowest concentration tested (0.01 μM), and continued to decrease to 0.02 ± 0.01 at 0.3 μM. At 1 Hz pacing, AP50 decreased from 307 ± 6 ms to 171 ± 18 ms at 0.03 μM as did AP90 from 407 ± 2 ms to 251 ± 22 ms before the spontaneous beat rate exceeded the pacing rate (Fig. 5B). The syncytium stopped beating at 1 μM nifedipine. The effects of additional Ca^{2+} channel effectors, verapamil and digoxin, are summarized in Table 1.

3.6. Cardiac Optopatch reports chronic drug effects on AP waveform

We next tested whether Optopatch reported effects from chronic drug exposure. Pentamidine causes prolonged QT and TdP in patients due to a reduction of hERG trafficking (Cordes et al., 2005; Kuryshev et al., 2005). We observed a gradual change in the AP waveform in the presence of pentamidine (Fig. 6). In the absence of pentamidine, beating was regular over the course of 44 h (Fig. 6A). At 1 μM pentamidine, CMs

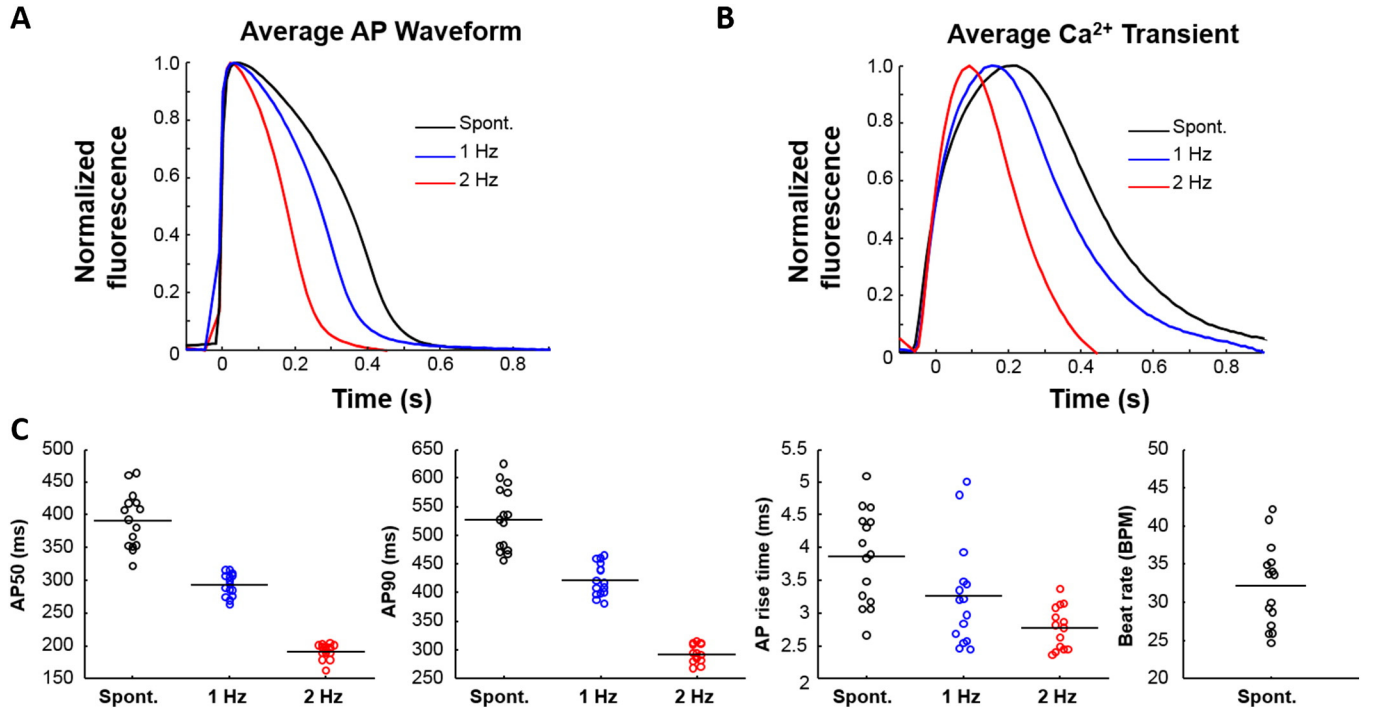

Fig. 3. Dish-to-dish variability of AP and CT parameters. (A) Average AP and (B) CT waveforms at spontaneous and paced regimes. (C) Dish-to-dish variability of AP and CT parameters before compound addition. Dot density plots for the AP50, AP90, AP rise time and spontaneous beat rate showing dish-to-dish variability across different beat rates. AP parameters show reduced variability with pacing, as indicated by the tighter clustering of data points. Black horizontal lines indicate the mean of the distributions.

showed no acute change in AP waveform (Fig. 6B). However, at 20 h, the AP waveform showed clear AP90 prolongation, and at 44 h, EADs were detected. At 10 μM pentamidine, we observed a dramatic AP90 prolongation after 20 h (Fig. 6C). Cells did not beat at 44 h. These measurements demonstrated that the Cardiac Optopatch system can probe long-term effects of drug exposure.

4. Discussion

Advances in drug screening for safety (Hardy, Lawrence, Standen, & Rodrigo, 2006; "International Conference on Harmonisation; guidance on S7B Nonclinical Evaluation of the Potential for Delayed Ventricular Repolarization (QT Interval Prolongation) by Human Pharmaceuticals; availability. Notice," *Federal Register*, 2005; Ma et al., 2011) and efficacy (Itzhaki et al., 2011; Yazawa et al., 2011), new stem cell-based therapies (Segers & Lee, 2008) and improved understanding of cardiac development (Panakova, Werdich, & Macrae, 2010) all necessitate new approaches to simultaneously measure voltage and calcium dynamics, with increased throughput, high dynamic range of spatio-temporal resolution and the ability to make both acute and chronic measurements *in vitro* and *in vivo* (Kaestner & Lipp, 2011; Leyton-Mange et al., 2014; Mandel et al., 2012). The CiPA initiative encourages creation of a more reliable assay to predict cardiac toxicity *in vivo*. One approach to cardiotoxicity screening is to use VSDs, which have been used to record AP waveforms from intact hearts since the 1970′s (Entcheva & Bien, 2006; Panakova et al., 2010; Salama & Morad, 1976), in cultured cardiomyocytes since the early 1990′s (Fast & Kleber, 1993; Windisch, Ahammer, Schaffer, Muller, & Platzer, 1995) and more recently from human iPSC-derived cardiomyocytes (Park, Lee, Tung, & Yue, 2014; Ren et al., 2011). However, dye-mediated phototoxicity is a concern and repeated imaging is a challenge. Dye-mediated phototoxicity is most acute for single-cell measurements, which require high magnification and consequently high illumination intensity.

Measurements of multiple modalities can distinguish among possible drug mechanisms of action. Simultaneous measurements with a VSD and a Ca^{2+} sensitive dye have been applied in intact guinea pig

Table 1
Summary of the effects of compound addition on select features of the action potential and calcium waveforms. For each drug, the concentration at which the observed physiological effect first occurred is listed. The symbols '↑20%' and '↓20%' indicate that the listed parameter increased or decreased by ~20%, respectively, relative to the addition of a 'blank' containing no drug. A dash mark (–) implies that no effect was observed. 'Stop beating' refers to the lowest concentration at which beating stops completely at both spontaneous beating and paced conditions in at least one field of view. Cells that did not adhere to the specified pace rate were omitted from consideration. Abbreviations: EADs, early after depolarizations; N/A, not applicable.

Compound	AP50 ↑20%	AP50 ↓20%	AP90 ↑20%	AP90 ↓20%	AP rise time ↑20%	EADs	Stop beating	Ca^{2+} amplitude ↑20%	Ca^{2+} Amplitude ↓20%	Ca^{2+} Flux stops	Ca^{2+} Sparks?
Quinidine	–	10 μM	1 μM	–	1 μM	3 μM	–	N/A	N/A	N/A	N/A
Lidocaine	10 μM	–	10 μM	–	10 μM	–	100 μM	N/A	N/A	N/A	N/A
Flecainide	1 μM	–	1 μM	–	1 μM	3 μM	10 μM	N/A	N/A	N/A	N/A
Amiodarone	–	–	–	–	–	–	–	N/A	N/A	N/A	N/A
E-4031	–	–	0.1 μM	–	0.03 μM	–	–	N/A	N/A	N/A	N/A
Verapamil	–	0.1 μM	–	0.1 μM	0.1 μM	–	1 μM	–	0.1 μM	1 μM	Yes
Nifedipine	–	0.01 μM	–	0.01 μM	0.01 μM	–	1 μM	–	0.01 μM	0.3 μM	Yes
Cisapride	–	–	0.01 μM	–	0.1 μM	1 μM	–	N/A	N/A	N/A	N/A
Digoxin	–	1 μM	1 μM	–	1 μM	–	3 μM	0.3 μM	1 μM	3 μM	Yes
Terfenadine	–	1 μM	–	–	1 μM	–	10 μM	N/A	N/A	N/A	N/A
Chromanol	–	–	–	–	–	–	–	N/A	N/A	N/A	N/A

Please cite this article as: Dempsey, G.T., et al., Cardiotoxicity screening with simultaneous optogenetic pacing, voltage imaging and calcium imaging, *Journal of Pharmacological and Toxicological Methods* (2016), http://dx.doi.org/10.1016/j.vascn.2016.05.003

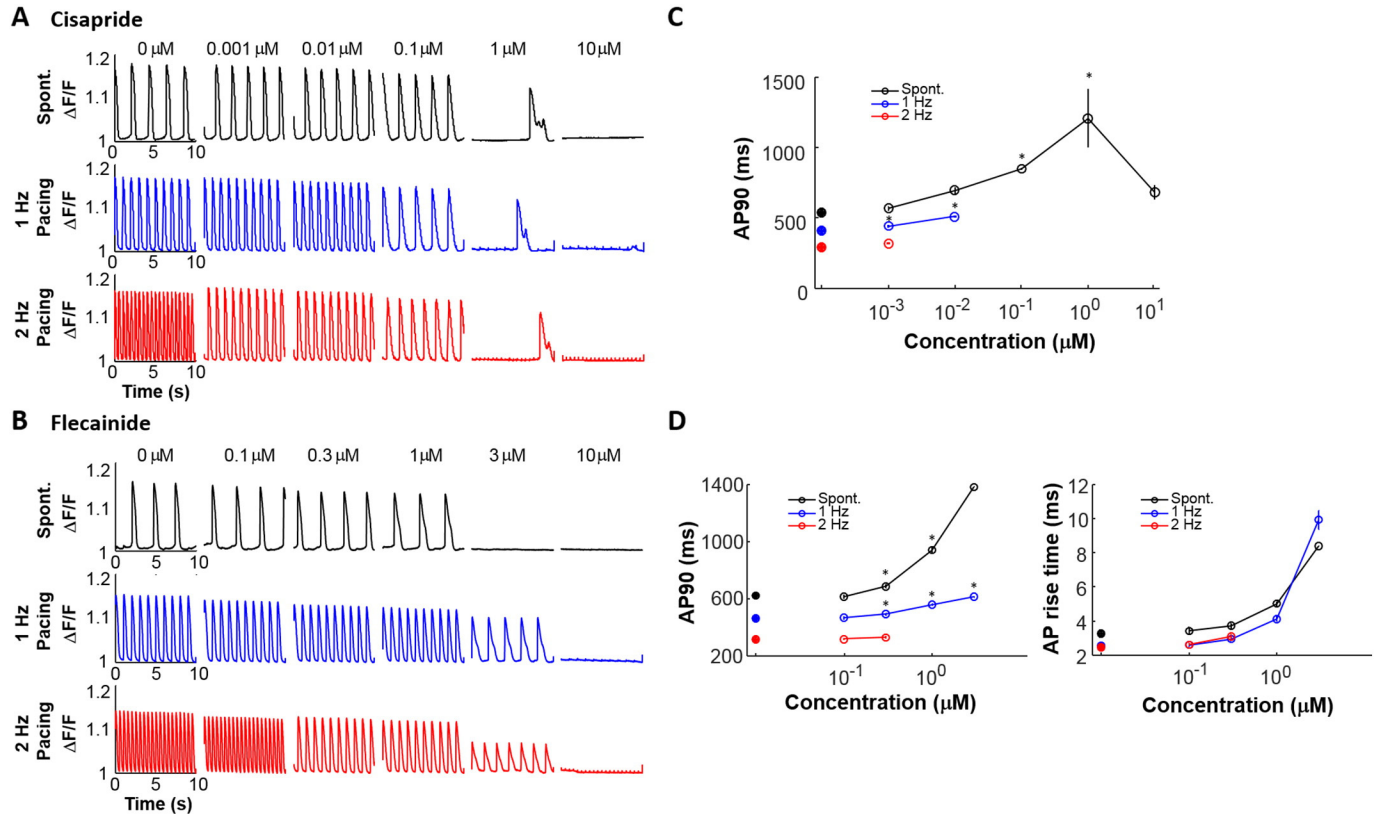

Fig. 4. Alterations in the AP waveform induced by cisapride and flecainide. Fluorescence (ΔF/F) *versus* time for (A) cisapride and (B) flecainide, for spontaneously beating cells (top, black), cells paced at 1 Hz (middle, blue) and 2 Hz (bottom, red). Cells were treated with sequentially increasing concentrations of drug. Cisapride induced EADs. (C) Change in AP90 as a function of cisapride concentration. (D) Change in AP90 and rise time as a function of flecainide concentration. (For interpretation of the references to color in this figure legend, the reader is referred to the web version of this article.)

hearts (Choi & Salama, 2000) and in centimeter-scale cultures of human iPSC-derived cardiomyocytes (Herron, Lee, & Jalife, 2012; P. Lee et al., 2012). Simultaneous measurement of voltage and Ca^{2+} with genetically encoded indicators has until recently been impossible due to the spectral overlap of GFP-based fluorescent proteins. The far red spectrum of the QuasArs resolves this challenge.

AP and CT waveforms are both highly sensitive to the beat rate. In spontaneously beating cultures, drugs can affect this rate, leading to

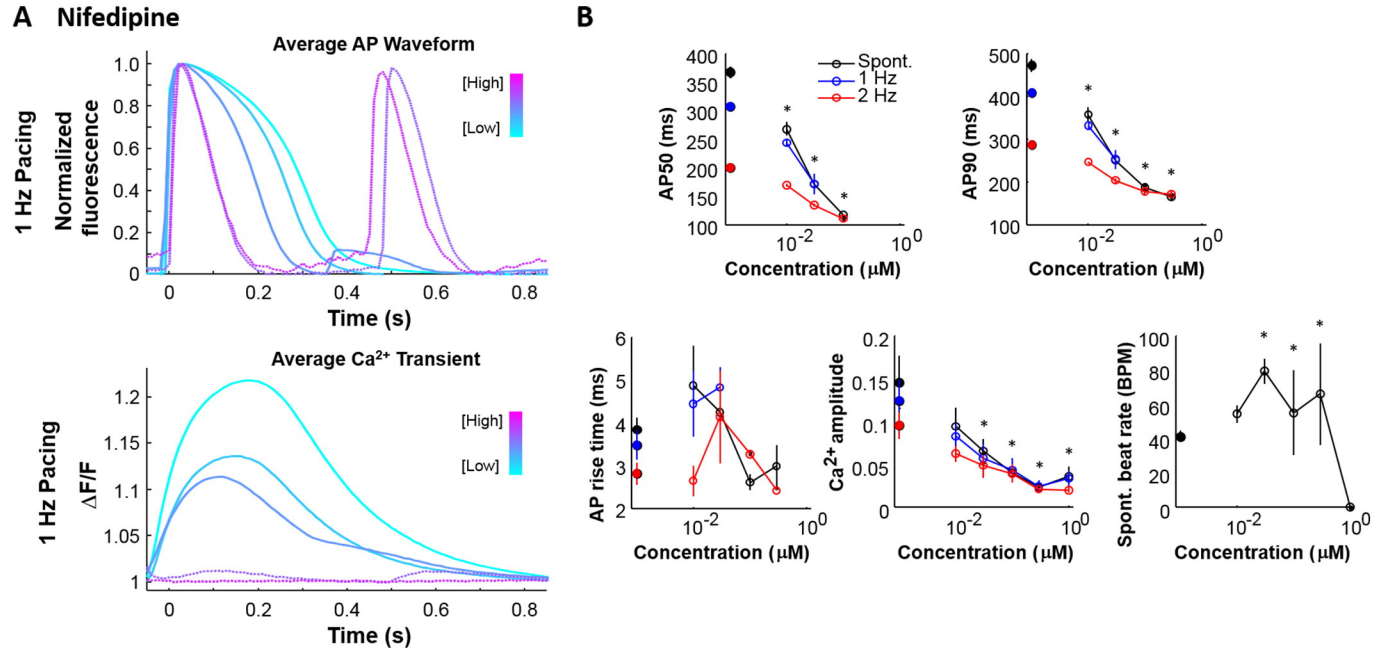

Fig. 5. Alterations in the AP waveform and Ca^{2+} transients induced by nifedipine. (A) Average normalized AP and (B) average (ΔF/F) CT waveforms at 1 Hz pacing for the nifedipine concentrations tested (cyan to magenta; lowest to highest concentration). (B) Quantification of the AP50, AP90, rise time, CT amplitude and spontaneous beat rate.

Please cite this article as: Dempsey, G.T., et al., Cardiotoxicity screening with simultaneous optogenetic pacing, voltage imaging and calcium imaging, *Journal of Pharmacological and Toxicological Methods* (2016), http://dx.doi.org/10.1016/j.vascn.2016.05.003

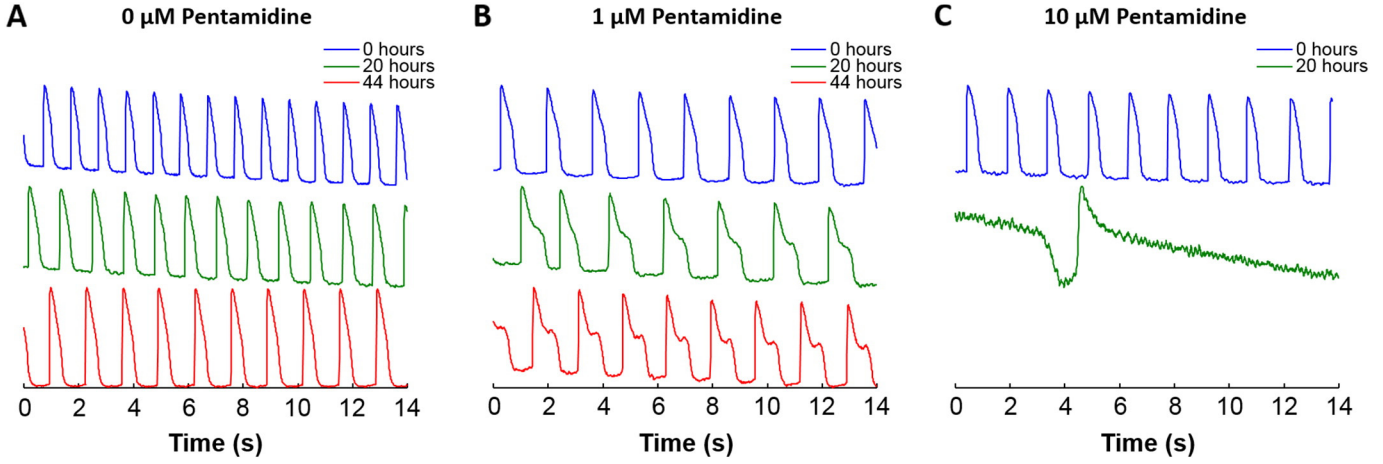

Fig. 6. Alterations in the AP waveform following chronic treatment with pentamidine. Fluorescence (ΔF/F) *versus* time at 0, 20 and 44 h after pentamidine addition.

changes in the waveform parameters that mask direct effects of the drug on particular ion channels. Pacing with field stimulation electrodes is standard practice, but risks contamination of the culture, a particular concern for long-term measurements. Combination of optogenetic pacing and voltage imaging has recently been achieved with a channelrhodopsin actuator and a red VSD (Park et al., 2014). The Cardiac Optopatch platform allows for a genetically encoded approach, which is desirable to alleviate concerns about phototoxicity and to enable cell type-specific labeling.

The Optopatch measurements precisely reflect the underlying AP and CT waveforms, but as with most optical assays, do not report absolute voltage or Ca^{2+}. Thus the assays are insensitive to perturbations that subtly shift the resting voltage or baseline Ca^{2+}. However, the cardiac action potential waveform is sensitive to resting membrane potential, and changes in APD are expected if compounds induce a shift in resting voltage. The calcium dynamics are reported with high signal-to-noise ratio by using a membrane-tethered GCaMP variant. Expression of the sensor at the plasma membrane has demonstrated faster dynamics than cytoplasmic versions, and furthermore reports Ca^{2+} sparks and waves. While these events were not the subject of our analysis, they were often seen in our movies.

Optopatch also offers a new dimension to testing delayed drug cardiotoxicity. Drugs with delayed cardiotoxic effects (Cordes et al., 2005; Kuryshev et al., 2005), (Molife et al., 2007) present a challenge for conventional hERG assays. The chronic measurements with pentamidine demonstrate the ability of the Optopatch assay to address this challenge. The assays performed here were performed on single-well cultures, but parallelization to multiple wells for higher throughput can be achieved through standard engineering measures.

In evaluating a prospective cardiotoxicity assay, one must distinguish between the measurement modality and the cellular substrate. As a substrate for cardiotoxicity screening, hiPSC-derived CMs replicate some, but not all physiological aspects of adult ventricular myocytes. Excitation-contraction coupling is a well-defined property of adult primary cardiomyocytes. Calcium mismanagement has been used in the past as a hallmark for pathology and maturity of cells. Within physiologically relevant pacing rates, the hiPSC-derived cardiomyocytes responded with action potential shortening upon increases in stimulation frequency, as do adult human myocytes. However, we observed a decrease in CT amplitude at elevated beat rate (Fig. 2), while an increase in CT amplitude at elevated beat rate has been reported for primary human atrial myocytes (Llach et al., 2011). Human embryonic stem cell-derived cardiomyocytes (hESC-CMs) showed expression of calcium handling proteins more similar to fetal than to adult ventricular myocytes, suggesting a mechanism for the difference in calcium transient morphology between the two (Liu, Fu, Siu, & Li, 2007). HiPSC-CMs exhibit a further suppression of amplitude and slower kinetics of the calcium transient than hESC-CMs, indicating an even greater immaturity of calcium handling (Y. K. Lee et al., 2011). A shift to a fetal gene expression pattern of calcium homeostatic proteins has been well characterized in failing human myocardium, supporting our hypothesis that the inverse calcium *vs.* frequency relationship observed in hiPSC-derived CMs is due to a lack of maturity and/or a similarity in phenotype to pathological heart tissue (Fisher, 1995).

Some compounds, including hERG, Na^+ and Ca^{2+} channel effectors, elicited responses which deviated from anticipated physiological responses. The increases in AP90 induced by cisapride and E-4031 are consistent with their mechanism as hERG blockers. EADs were observed for cisapride but only occasionally for E-4031. E-4031 is a commonly used positive control, with potent and selective hERG blocking properties. Canine *in vivo* and purkinje fiber studies using E-4031 have shown APD prolongation at concentrations ranging from <1 nM–30 nM, respectively (Faivre, Forest, Gout, & Bril, 1999; Webster et al., 2001). Our results observed significant APD prolongation at 100 nM, a higher concentration than reported by others using similar hiPSC-CMs. For example, Peng et al. and Ma et al. reported a ≥66% prolongation of APD90 at 30 nM in electrically paced cells (1 Hz), with subsequent EADs at 100 nM in spontaneous or slower paced cells (0.5 Hz) (Ma et al., 2011; Peng, Lacerda, Kirsch, Brown, & Bruening-Wright, 2010). Non-invasive MEA measurements on hiPSC-CMs reported arrhythmic activity at concentrations ≥10 nM (Guo et al., 2013; Harris et al., 2013; Nakamura et al., 2014). The recent observation that AP waveform depends on plating density (Du et al., 2015) suggests that this variable, not standardized between research groups, may explain some of the variability within the literature and the different results obtained here. The paucity of data on cells from the same source, studied on the same platform, under identical conditions makes it difficult to form a consensus on pharmacological effects.

In the case of Na^+ channel block, both anticipated and unanticipated effects were observed. Flecainide and quinidine showed an increase in rise time consistent with their mechanism as Class Ia Na^+ channel blockers and led to EADs at 1 and 3 μM, respectively. E-4031 also increased AP rise time, suggesting an interaction with cardiac sodium channels in addition to its known action on hERG. Alternatively, a depolarizing shift in the resting membrane potential has been observed for selective hERG blockers, which may induce similar sodium channel inactivation-dependent shifts in rise time (Gibson, Yue, Bronson, Palmer, & Numann, 2014; Ma et al., 2011). Frequency-dependent increases in rise time were not observed across drugs tested and most preparations did not respond to 2 Hz pacing after exposure to Na^+ channel blockers. Inability to respond to increased pacing may be, in part, due to the frequency-dependent increase in sodium channel potency observed for Class 1 exhibiting compounds.

Please cite this article as: Dempsey, G.T., et al., Cardiotoxicity screening with simultaneous optogenetic pacing, voltage imaging and calcium imaging, *Journal of Pharmacological and Toxicological Methods* (2016), http://dx.doi.org/10.1016/j.vascn.2016.05.003

Ca^{2+} modulators produced the expected drug effects. Decreases in CT amplitude for nifedipine and verapamil are consistent with their mechanism as L-type Ca^{2+} channel blockers, while the increase in CT amplitude for digoxin is consistent with its mechanism as a positive inotrope.

For most compounds tested (with the exception of chromanol and amiodarone), we observed a dose-dependent reduction in the signal amplitude. Cisapride, for example, showed a decrease in signal amplitude between 0 and 0.1 μM of 14%. At the highest concentration, we observed EADs and a decrease in the signal amplitude by 30% relative to no drug added. Measurements of photostability establish that photobleaching is responsible for a negligible portion of this decrement in signal amplitude. Thus it is likely that the reductions in signal amplitude reflect real changes in the membrane voltage. Nifedipine, for example, showed a dramatic reduction in both the Ca^{2+} and voltage amplitudes with increasing dose (Fig. 5B). The block of Ca^{2+} channels by nifedipine leads to an increase in the beat rate and a reduction in the AP amplitude that correlates well with the reduction in Ca^{2+} amplitude. These effects are consistent with nifedipine's mechanism of action.

Lastly, some compounds showed no effect upon addition to iPSC-derived CMs. The absence of responses to chromanol implies that the cells lack a substantial I_{ks} current, likely a consequence of the immaturity of these cells. The lack of effects of amiodarone are more difficult to reconcile. Amiodarone is commonly prescribed as an antiarrhythmic, as it exhibits sodium (15.9 μM), calcium (1.9 μM) and hERG (0.86 μM) block to varying degrees (Kramer et al., 2013). Clinically, amiodarone has been associated with "slowed sinus nodal discharge rate, lengthened A–V nodal conduction time, increased atrial and ventricular monophasic action potential duration and refractory periods." (Zipes & Troup, 1978). A study in hiPSC-CMs reported a reduction in spontaneous beat rate up to 100 μM (Yokoo et al., 2009), while a similar study reported significant increases in beat rate from 1 to 10 μM (Mehta et al., 2013). In the present study, we observed no effect on AP duration, rise time or spontaneous beat rate from 0.3–3.0 μM, which compares well to a recent study by Gilchrist et.al. (Gilchrist, Lewis, Gay, Sellgren, & Grego, 2015). Thus the effects of amiodarone are quite variable in hiPSC-CM platforms and require further investigation. Additional work with a broader array of compounds will be required to develop a detailed map of drug effects *in vitro* to clinical outcomes *in vivo*.

Our study, as well as others in the literature, has confirmed the heterogeneous population of cardiomyocytes present in hiPSC-derived CMs (Fig. 1). The cardiomyocytes used for this study are claimed to be >95% pure according to the manufacturer's specifications, with relative contributions of 50% ventricular, 25% atrial and 25% nodal cells. As is the case in the human heart, regional differences in pharmacology have been observed and often serve as the basis for specificity of drugs. For example, atrial-selective drugs exploit the presence of Kv1.5 and the relatively depolarized membrane potential (Ravens, Poulet, Wettwer, & Knaut, 2013). Because our current analysis captures APs from a discrete population of cells, it is plausible that differences in pharmacology observed arise from statistical averaging over the mixed population. Future work will entail the design of cell-type specific vectors for targeted expression in either ventricular, atrial or nodal cell populations, a capability uniquely afforded by genetically encoded indicators.

These data demonstrate that the Optopatch technology provides a means to non-invasively study hiPSC-derived cardiomyocytes to better characterize their native phenotype and the cardiotoxic effects of novel chemical entities. The use of fluorescent proteins to study complex electrophysiology is also amenable to increased throughput using automation and multi-well plate based platforms, providing increased flexibility to capture myocyte physiology. The ability to pace the CMs reduces the rate-dependent changes in AP and CT waveforms, which would otherwise mask the effects of many compounds. Differences in some pharmacological responses within the literature and between the literature and the present measurements highlight the importance of defining standard cell culture and measurement conditions. This platform should prove useful in reaching one of the major goals of the CiPA initiative, namely an *in vitro* assay with hiPSC-derived CMs for the accurate reporting of cardiotoxic effects of drug compounds.

Author contributions

GTD, KWC, BSB, JDM, JMK, and AEC designed the study. GTD, NA, CN and JMK performed all cell culturing, transductions and drug preparations. GTD and JMK built the instrument and performed all measurements. GTD, KWC and JMK performed all analyses. GTD, KWC and JMK wrote the manuscript. AEC contributed to sensor design prior to work performed at Q-State Biosciences.

Ethical approval

None required.

Funding information

AEC and JMK were partially supported by PECASE award N00014-11-1-0549 and US National Institutes of Health grants 1-R01-EB012498 and New Innovator grant 1-DP2-OD007428.

Conflict of interest

JMK and AEC are co-founders of Q-State Biosciences. GTD, NA and CN are affiliated with Q-State Biosciences. KWC and BSB are affiliated with GlaxoSmithKline Safety Assessment. JDM is affiliated with GlaxoSmithKline Alternative Discovery and Development.

Acknowledgments

We thank K. Eggan, D. Margulies, K. Werley and C. Hechard for their helpful discussions.

References

Adams, C. P., & Brantner, V. V. (2010). Spending on new drug development1. *Health Economics*, *19*, 130–141.

Burridge, P. W., Matsa, E., Shukla, P., Lin, Z. C., Churko, J. M., Ebert, A. D., ... Wu, J. C. (2014). Chemically defined generation of human cardiomyocytes. *Nature Methods*, *11*, 855–860.

Caspi, O., Itzhaki, I., Kehat, I., Gepstein, A., Arbel, G., Huber, I., ... Gepstein, L. (2009). In vitro electrophysiological drug testing using human embryonic stem cell derived cardiomyocytes. *Stem Cells and Development*, *18*, 161–172.

Cavero, I., & Holzgrefe, H. (2014). Comprehensive in vitro proarrhythmia assay, a novel in vitro/in silico paradigm to detect ventricular proarrhythmic liability: A visionary 21st century initiative. *Expert Opinion on Drug Safety*, *13*, 745–758.

Chen, T. W., Wardill, T. J., Sun, Y., Pulver, S. R., Renninger, S. L., Baohan, A., ... Kim, D. S. (2013). Ultrasensitive fluorescent proteins for imaging neuronal activity. *Nature*, *499*, 295–300.

Choi, B. R., & Salama, G. (2000). Simultaneous maps of optical action potentials and calcium transients in guinea-pig hearts: Mechanisms underlying concordant alternans. *The Journal of Physiology*, *529*(Pt 1), 171–188.

Chouabe, C., Drici, M. D., Romey, G., Barhanin, J., & Lazdunski, M. (1998). HERG and KvLQT1/IsK, the cardiac K^+ channels involved in long QT syndromes, are targets for calcium channel blockers. *Molecular Pharmacology*, *54*, 695–703.

Cordes, J. S., Sun, Z., Lloyd, D. B., Bradley, J. A., Opsahl, A. C., Tengowski, M. W., ... Zhou, J. (2005). Pentamidine reduces hERG expression to prolong the QT interval. *British Journal of Pharmacology*, *145*, 15–23.

Coumel, P., Leclercq, J. F., & Lucet, V. (1985). Possible mechanisms of the arrhythmias in the long QT syndrome. *European Heart Journal*, *6*(Suppl. D), 115–129.

De Ponti, F., Poluzzi, E., Cavalli, A., Recanatini, M., & Montanaro, N. (2002). Safety of non-antiarrhythmic drugs that prolong the QT interval or induce torsade de pointes: An overview. *Drug Safety: an International Journal of Medical Toxicology and Drug Experience*, *25*, 263–286.

Doevendans, P. A., Kubalak, S. W., An, R. H., Becker, D. K., Chien, K. R., & Kass, R. S. (2000). Differentiation of cardiomyocytes in floating embryoid bodies is comparable to fetal cardiomyocytes. *Journal of Molecular and Cellular Cardiology*, *32*, 839–851.

Du, D. T., Hellen, N., Kane, C., & Terracciano, C. M. (2015). Action potential morphology of human induced pluripotent stem cell-derived cardiomyocytes does not predict cardiac chamber specificity and is dependent on cell density. *Biophysical Journal*, *108*, 1–4.

Entcheva, E., & Bien, H. (2006). Macroscopic optical mapping of excitation in cardiac cell networks with ultra-high spatiotemporal resolution. *Progress in Biophysics and Molecular Biology*, *92*, 232–257.

Please cite this article as: Dempsey, G.T., et al., Cardiotoxicity screening with simultaneous optogenetic pacing, voltage imaging and calcium imaging, *Journal of Pharmacological and Toxicological Methods* (2016), http://dx.doi.org/10.1016/j.vascn.2016.05.003

Faivre, J. F., Forest, M. C., Gout, B., & Bril, A. (1999). Electrophysiological characterization of BRL-32872 in canine Purkinje fiber and ventricular muscle. Effect on early after-depolarizations and repolarization dispersion. *European Journal of Pharmacology*, *383*, 215–222.

Fast, V. G., & Kleber, A. G. (1993). Microscopic conduction in cultured strands of neonatal rat heart cells measured with voltage-sensitive dyes. *Circulation Research*, *73*, 914–925.

International conference on harmonisation; guidance on S7B nonclinical evaluation of the potential for delayed ventricular repolarization (QT interval prolongation) by human pharmaceuticals; availability. Notice. *Federal Register*, *70*(2005)., 61133–61134.

Fisher, D. J. (1995). Recent insights into the regulation of cardiac Ca^{2+} flux during perinatal development and in cardiac failure. *Current Opinion in Cardiology*, *10*, 44–51.

Gibson, J. K., Yue, Y., Bronson, J., Palmer, C., & Numann, R. (2014). Human stem cell-derived cardiomyocytes detect drug-mediated changes in action potentials and ion currents. *Journal of Pharmacological and Toxicological Methods*, *70*, 255–267.

Gilchrist, K. H., Lewis, G. F., Gay, E. A., Sellgren, K. L., & Grego, S. (2015). High-throughput cardiac safety evaluation and multi-parameter arrhythmia profiling of cardiomyocytes using microelectrode arrays. *Toxicology and Applied Pharmacology*, *288*, 249–257.

Gintant, G. (2011). An evaluation of hERG current assay performance: Translating preclinical safety studies to clinical QT prolongation. *Pharmacology & Therapeutics*, *129*, 109–119.

Guengerich, F. P. (2011). Mechanisms of drug toxicity and relevance to pharmaceutical development. *Drug Metabolism and Pharmacokinetics*, *26*, 3–14.

Guo, L., Coyle, L., Abrams, R. M., Kemper, R., Chiao, E. T., & Kolaja, K. L. (2013). Refining the human iPSC-cardiomyocyte arrhythmic risk assessment model. *Toxicological Sciences*, *136*, 581–594.

Guo, L., Qian, J. Y., Abrams, R., Tang, H. M., Weiser, T., Sanders, M. J., & Kolaja, K. L. (2011). The electrophysiological effects of cardiac glycosides in human iPSC-derived cardiomyocytes and in guinea pig isolated hearts. *Cellular Physiology and Biochemistry: Internation Journal of Experimental Cellular Physiology, Biochemistry, and Pharmacology*, *27*, 453–462.

Hanson, L. A., Bass, A. S., Gintant, G., Mittelstadt, S., Rampe, D., & Thomas, K. (2006). ILSI-HESI cardiovascular safety subcommittee initiative: Evaluation of three non-clinical models of QT prolongation. *Journal of Pharmacological and Toxicological Methods*, *54*, 116–129.

Hardy, M. E., Lawrence, C. L., Standen, N. B., & Rodrigo, G. C. (2006). Can optical recordings of membrane potential be used to screen for drug-induced action potential prolongation in single cardiac myocytes? *Journal of Pharmacological and Toxicological Methods*, *54*, 173–182.

Harris, K., Aylott, M., Cui, Y., Louttit, J. B., McMahon, N. C., & Sridhar, A. (2013). Comparison of electrophysiological data from human-induced pluripotent stem cell-derived cardiomyocytes to functional preclinical safety assays. *Toxicological Sciences*, *134*, 412–426.

Haverkamp, W., Breithardt, G., Camm, A. J., Janse, M. J., Rosen, M. R., Antzelevitch, C., ... Shah, R. (2000). The potential for QT prolongation and pro-arrhythmia by non-anti-arrhythmic drugs: clinical and regulatory implications. Report on a policy conference of the European Society of Cardiology. *Cardiovascular Research*, *47*, 219–233.

He, J. Q., Ma, Y., Lee, Y., Thomson, J. A., & Kamp, T. J. (2003). Human embryonic stem cells develop into multiple types of cardiac myocytes: Action potential characterization. *Circulation Research*, *93*, 32–39.

Hennessy, S., Leonard, C. E., Newcomb, C., Kimmel, S. E., & Bilker, W. B. (2008). Cisapride and ventricular arrhythmia. *British Journal of Clinical Pharmacology*, *66*, 375–385.

Herron, T. J., Lee, P., & Jalife, J. (2012). Optical imaging of voltage and calcium in cardiac cells & tissues. *Circulation Research*, *110*, 609–623.

Himmel, H. M. (2013). Drug-induced functional cardiotoxicity screening in stem cell-derived human and mouse cardiomyocytes: Effects of reference compounds. *Journal of Pharmacological and Toxicological Methods*, *68*, 97–111.

Hochbaum, D. R., Zhao, Y., Farhi, S. L., Klapoetke, N., Werley, C. A., Kapoor, V., ... Cohen, A. E. (2014). All-optical electrophysiology in mammalian neurons using engineered microbial rhodopsins. *Nature Methods*, *11*, 825–833.

Holzgrefe, H., Ferber, G., Champeroux, P., Gill, M., Honda, M., Greiter-Wilke, A., ... Saulnier, M. (2014). Preclinical QT safety assessment: Cross-species comparisons and human translation from an industry consortium. *Journal of Pharmacological and Toxicological Methods*, *69*, 61–101.

Honda, M., Kiyokawa, J., Tabo, M., & Inoue, T. (2011). Electrophysiological characterization of cardiomyocytes derived from human induced pluripotent stem cells. *Journal of Pharmacological Sciences*, *117*, 149–159.

Hou, J. H., Kralj, J. M., Douglass, A. D., Engert, F., & Cohen, A. E. (2014). Simultaneous mapping of membrane voltage and calcium in zebrafish heart in vivo reveals chamber-specific developmental transitions in ionic currents. *Frontiers in Physiology*, *5*, 344.

Huebsch, N., Loskill, P., Mandegar, M. A., Marks, N. C., Sheehan, A. S., Ma, Z., ... Healy, K. E. (2014). Automated video-based analysis of contractility and calcium flux in human iPS-derived cardiomyocytes cultured over different spatial scales. *Tissue Engineering. Part C, Methods*.

ICHS7B (2005). Nonclinical testing for effect on ventricular repolarization. http://www.ich.org/cache/compo/276-254-1.htmlhttp://www.emea.eu.int/htms/human/ich/safety/ichdraft.htm (online)

Itzhaki, I., Maizels, L., Huber, I., Zwi-Dantsis, L., Caspi, O., Winterstern, A., ... Gepstein, L. (2011). Modelling the long QT syndrome with induced pluripotent stem cells. *Nature*, *471*, 225–229.

Kaestner, L., & Lipp, P. (2011). Screening action potentials: The power of light. *Frontiers in Pharmacology*, *2*, 42.

Kaestner, L., Scholz, A., Tian, Q., Ruppenthal, S., Tabellion, W., Wiesen, K., ... Lipp, P. (2014). Genetically encoded Ca^{2+} indicators in cardiac myocytes. *Circulation Research*, *114*, 1623–1639.

Keating, M. T. (1995). Molecular genetics of long QT syndrome. *Society of General Physiologists Series*, *50*, 53–60.

Kramer, J., Obejero-Paz, C. A., Myatt, G., Kuryshev, Y. A., Bruening-Wright, A., Verducci, J. S. , & Brown, A. M. (2013). MICE models: Superior to the HERG model in predicting Torsade de Pointes. *Scientific Reports*, *3*, 2100.

Kuryshev, Y. A., Ficker, E., Wang, L., Hawryluk, P., Dennis, A. T., Wible, B. A., ... Rampe, D. (2005). Pentamidine-induced long QT syndrome and block of hERG trafficking. *The Journal of Pharmacology and Experimental Therapeutics*, *312*, 316–323.

Lan, F., Lee, A. S., Liang, P., Sanchez-Freire, V., Nguyen, P. K., Wang, L., ... Wu, J. C. (2013). Abnormal calcium handling properties underlie familial hypertrophic cardiomyopathy pathology in patient-specific induced pluripotent stem cells. *Cell Stem Cell*, *12*, 101–113.

Lee, P., Klos, M., Bollensdorff, C., Hou, L., Ewart, P., Kamp, T. J., ... Herron, T. J. (2012). Simultaneous voltage and calcium mapping of genetically purified human induced pluripotent stem cell-derived cardiac myocyte monolayers. *Circulation Research*, *110*, 1556–1563.

Lee, Y. K., Ng, K. M., Lai, W. H., Chan, Y. C., Lau, Y. M., Lian, Q., ... Siu, C. W. (2011). Calcium homeostasis in human induced pluripotent stem cell-derived cardiomyocytes. *Stem Cell Reviews*, *7*, 976–986.

Leyton-Mange, J. S., Mills, R. W., Macri, V. S., Jang, M. Y., Butte, F. N., Ellinor, P. T., & Milan, D. J. (2014). Rapid cellular phenotyping of human pluripotent stem cell-derived cardiomyocytes using a genetically encoded fluorescent voltage sensor. *Stem Cell Reports*, *2*, 163–170.

Liu, J., Fu, J. D., Siu, C. W., & Li, R. A. (2007). Functional sarcoplasmic reticulum for calcium handling of human embryonic stem cell-derived cardiomyocytes: Insights for driven maturation. *Stem Cells*, *25*, 3038–3044.

Llach, A., Molina, C. E., Fernandes, J., Padro, J., Cinca, J., & Hove-Madsen, L. (2011). Sarcoplasmic reticulum and L-type $Ca(2)(+)$ channel activity regulate the beat-to-beat stability of calcium handling in human atrial myocytes. *The Journal of Physiology*, *589*, 3247–3262.

Lu, H. R., Vlaminckx, E., Hermans, A. N., Rohrbacher, J., Van Ammel, K., Towart, R., ... Gallacher, D. J. (2008). Predicting drug-induced changes in QT interval and arrhythmias: QT-shortening drugs point to gaps in the ICHS7B guidelines. *British Journal of Pharmacology*, *154*, 1427–1438.

Ma, J., Guo, L., Fiene, S. J., Anson, B. D., Thomson, J. A., Kamp, T. J., ... January, C. T. (2011). High purity human-induced pluripotent stem cell-derived cardiomyocytes: Electrophysiological properties of action potentials and ionic currents. *American Journal of Physiology. Heart and Circulatory Physiology*, *301*, H2006–H2017.

Maclaurin, D., Venkatachalam, V., Lee, H., & Cohen, A. E. (2013). Mechanism of voltage-sensitive fluorescence in a microbial rhodopsin. *Proceedings of the National Academy of Sciences of the United States of America*, *110*, 5939–5944.

Mandel, Y., Weissman, A., Schick, R., Barad, L., Novak, A., Meiry, G., ... Binah, O. (2012). Human embryonic and induced pluripotent stem cell-derived cardiomyocytes exhibit beat rate variability and power-law behavior. *Circulation*, *125*, 883–893.

Mehta, A., Chung, Y., Sequiera, G. L., Wong, P., Liew, R., & Shim, W. (2013). Pharmacoelectrophysiology of viral-free induced pluripotent stem cell-derived human cardiomyocytes. *Toxicological Sciences*, *131*, 458–469.

Miller, E. W., Lin, J. Y., Frady, E. P., Steinbach, P. A., Kristan, W. B., Jr., & Tsien, R. Y. (2012). Optically monitoring voltage in neurons by photo-induced electron transfer through molecular wires. *Proceedings of the National Academy of Sciences of the United States of America*, *109*, 2114–2119.

Molife, R., Fong, P., Scurr, M., Judson, I., Kaye, S., & de Bono, J. (2007). HDAC inhibitors and cardiac safety. *Clinical Cancer Research: An Official Journal of the American Association for Cancer Research*, *13*, 1068 (author reply 1068–1069).

Mummery, C., Ward-van Oostwaard, D., Doevendans, P., Spijker, R., van den Brink, S., Hassink, R., ... Tertoolen, L. (2003). Differentiation of human embryonic stem cells to cardiomyocytes: Role of coculture with visceral endoderm-like cells. *Circulation*, *107*, 2733–2740.

Nakamura, Y., Matsuo, J., Miyamoto, N., Ojima, A., Ando, K., Kanda, Y., ... Sekino, Y. (2014). Assessment of testing methods for drug-induced repolarization delay and arrhythmias in an iPS cell-derived cardiomyocyte sheet: Multi-site validation study. *Journal of Pharmacological Sciences*, *124*, 494–501.

Olson, H., Betton, G., Robinson, D., Thomas, K., Monro, A., Kolaja, G., ... Heller, A. (2000). Concordance of the toxicity of pharmaceuticals in humans and in animals. *Regulatory Toxicology and Pharmacology*, *32*, 56–67.

Panakova, D., Werdich, A. A., & Macrae, C. A. (2010). Wnt11 patterns a myocardial electrical gradient through regulation of the L-type $Ca(2+)$ channel. *Nature*, *466*, 874–878.

Park, S. A., Lee, S. R., Tung, L., & Yue, D. T. (2014). Optical mapping of optogenetically shaped cardiac action potentials. *Scientific Reports*, *4*, 6125.

Peng, S., Lacerda, A. E., Kirsch, G. E., Brown, A. M., & Bruening-Wright, A. (2010). The action potential and comparative pharmacology of stem cell-derived human cardiomyocytes. *Journal of Pharmacological and Toxicological Methods*, *61*, 277–286.

Puppala, D., Collis, L. P., Sun, S. Z., Bonato, V., Chen, X., Anson, B., ... Engle, S. J. (2013). Comparative gene expression profiling in human-induced pluripotent stem cell-derived cardiocytes and human and cynomolgus heart tissue. *Toxicological Sciences*, *131*, 292–301.

Ravens, U., Poulet, C., Wettwer, E., & Knaut, M. (2013). Atrial selectivity of antiarrhythmic drugs. *The Journal of Physiology*, *591*, 4087–4097.

Redfern, W. S., Carlsson, L., Davis, A. S., Lynch, W. G., MacKenzie, I., Palethorpe, S., ... Hammond, T. G. (2003). Relationships between preclinical cardiac electrophysiology, clinical QT interval prolongation and torsade de pointes for a broad range of drugs: Evidence for a provisional safety margin in drug development. *Cardiovascular Research*, *58*, 32–45.

Ren, Y., Lee, M. Y., Schliffke, S., Paavola, J., Amos, P. J., Ge, X., ... Qyang, Y. (2011). Small molecule Wnt inhibitors enhance the efficiency of BMP-4-directed cardiac differentiation of human pluripotent stem cells. *Journal of Molecular and Cellular Cardiology*, *51*, 280–287.

Please cite this article as: Dempsey, G.T., et al., Cardiotoxicity screening with simultaneous optogenetic pacing, voltage imaging and calcium imaging, *Journal of Pharmacological and Toxicological Methods* (2016), http://dx.doi.org/10.1016/j.vascn.2016.05.003

Ribeiro, M. C., Tertoolen, L. G., Guadix, J. A., Bellin, M., Kosmidis, G., D'Aniello, C., ... Passier, R. (2015). Functional maturation of human pluripotent stem cell derived cardiomyocytes in vitro-correlation between contraction force and electrophysiology. *Biomaterials*, *51*, 138–150.

Roden, D. M., Lazzara, R., Rosen, M., Schwartz, P. J., Towbin, J., & Vincent, G. M. (1996). Multiple mechanisms in the long-QT syndrome. Current knowledge, gaps, and future directions. The SADS foundation task force on LQTS. *Circulation*, *94*, 1996–2012.

Sager, P. T., Gintant, G., Turner, J. R., Pettit, S., & Stockbridge, N. (2014). Rechanneling the cardiac proarrhythmia safety paradigm: A meeting report from the cardiac safety research consortium. *American Heart Journal*, *167*, 292–300.

Salama, G., & Morad, M. (1976). Merocyanine 540 as an optical probe of transmembrane electrical activity in the heart. *Science*, *191*, 485–487.

Sanguinetti, M. C., Jiang, C., Curran, M. E., & Keating, M. T. (1995). A mechanistic link between an inherited and an acquired cardiac arrhythmia: HERG encodes the IKr potassium channel. *Cell*, *81*, 299–307.

Schram, G., Zhang, L., Derakhchan, K., Ehrlich, J. R., Belardinelli, L., & Nattel, S. (2004). Ranolazine: Ion-channel-blocking actions and in vivo electrophysiological effects. *British Journal of Pharmacology*, *142*, 1300–1308.

Segers, V. F., & Lee, R. T. (2008). Stem-cell therapy for cardiac disease. *Nature*, *451*, 937–942.

Shang, W., Lu, F., Sun, T., Xu, J., Li, L. L., Wang, Y., ... Cheng, H. (2014). Imaging Ca^{2+} nanosparks in heart with a new targeted biosensor. *Circulation Research*, *114*, 412–420.

Song, Y., Shryock, J. C., Wu, L., & Belardinelli, L. (2004). Antagonism by ranolazine of the pro-arrhythmic effects of increasing late INa in guinea pig ventricular myocytes. *Journal of Cardiovascular Pharmacology*, *44*, 192–199.

Stevens, J. L., & Baker, T. K. (2009). The future of drug safety testing: Expanding the view and narrowing the focus. *Drug Discovery Today*, *14*, 162–167.

Vanderlaan, R. D., Oudit, G. Y., & Backx, P. H. (2003). Electrophysiological profiling of cardiomyocytes in embryonic bodies derived from human embryonic stem cells: Therapeutic implications. *Circulation Research*, *93*, 1–3.

Wang, G., McCain, M. L., Yang, L., He, A., Pasqualini, F. S., Agarwal, A., ... Pu, W. T. (2014). Modeling the mitochondrial cardiomyopathy of Barth syndrome with induced pluripotent stem cell and heart-on-chip technologies. *Nature Medicine*, *20*, 616–623.

Webster, R., Allan, G., Anto-Awuakye, K., Harrison, A., Kidd, T., Leishman, D., ... Walker, D. (2001). Pharmacokinetic/pharmacodynamic assessment of the effects of E4031, cisapride, terfenadine and terodiline on monophasic action potential duration in dog. *Xenobiotica*, *31*, 633–650.

Windisch, H., Ahammer, H., Schaffer, P., Muller, W., & Platzer, D. (1995). Optical multisite monitoring of cell excitation phenomena in isolated cardiomyocytes. *Pflügers Archiv*, *430*, 508–518.

Yazawa, M., Hsueh, B., Jia, X., Pasca, A. M., Bernstein, J. A., Hallmayer, J., & Dolmetsch, R. E. (2011). Using induced pluripotent stem cells to investigate cardiac phenotypes in Timothy syndrome. *Nature*, *471*, 230–234.

Yokoo, N., Baba, S., Kaichi, S., Niwa, A., Mima, T., Doi, H., Yamanaka, S., Nakahata, T., & Heike, T. (2009). The effects of cardioactive drugs on cardiomyocytes derived from human induced pluripotent stem cells. *Biochemical and Biophysical Research Communications*, *387*, 482–488.

Zhou, Z., Gong, Q., Ye, B., Fan, Z., Makielski, J. C., Robertson, G. A., & January, C. T. (1998). Properties of HERG channels stably expressed in HEK 293 cells studied at physiological temperature. *Biophysical Journal*, *74*, 230–241.

Zipes, D. P., & Troup, P. J. (1978). New antiarrhythmic agents: Amiodarone, aprindine, disopyramide, ethmozin, mexiletine, tocainide, verapamil. *The American Journal of Cardiology*, *41*, 1005–1024.

Please cite this article as: Dempsey, G.T., et al., Cardiotoxicity screening with simultaneous optogenetic pacing, voltage imaging and calcium imaging, *Journal of Pharmacological and Toxicological Methods* (2016), http://dx.doi.org/10.1016/j.vascn.2016.05.003